ACS APPLIED ELECTRONIC MATERIALS

Article

Cite This: ACS Appl. Electron. Mater. 2019, 1, 1641−1652

pubs.acs.org/acsaelm

Interfacial Properties of Doped Semiconductor Materials Can Alter the Behavior of *Pseudomonas aeruginosa* Films

Alexey V. Gulyuk,[†] Dennis R. LaJeunesse,[‡] Pramod Reddy,[§] Ronny Kirste,[§] Ramon Collazo,[†] and Albena Ivanisevic*[,†]

[†]Department of Materials Science and Engineering, North Carolina State University, Raleigh, North Carolina 27695, United States

[‡]Department of Nanoscience, Joint School of Nanoscience and Nanoengineering, University of North Carolina at Greensboro, Greensboro, North Carolina 27401, United States

[§]Adroit Materials, 2054 Kildaire Farm Rd., Suite 205, Cary, North Carolina 27518, United States

Supporting Information

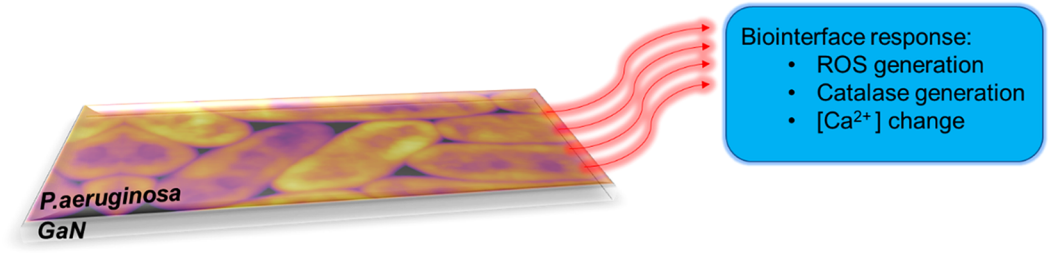

ABSTRACT: A simple treatment of UV light exposure can change the interfacial properties of variably doped GaN substrates. The changes in surface charge and chemistry after exposure to UV light were studied as way to alter the behavior of *Pseudomonas aeruginosa* films. The properties of GaN surfaces were characterized by atomic force microscopy, Kelvin probe force microscopy, and X-ray photoelectron spectroscopy. The *Pseudomonas aeruginosa* film responses were quantified by analyzing changes in the amount of catalase, reactive oxygen species, and intracellular Ca^{2+} concentrations. The comprehensive analysis supports the notion that the response of *P. aeruginosa* biofilms can be controlled by the properties of the interface and the amount of time the film is in contact with it.

KEYWORDS: *gallium nitride, Pseudomonas aeruginosa, UV light, X-ray photoelectron spectroscopy, Kelvin probe force microscopy, reactive oxygen species, catalase, intracellular Ca^{2+}*

1. INTRODUCTION

UV light treatments have found a broad range of applications in different spheres of human life: manufacturing, healthcare, forensic science, agriculture, and natural sciences and engineering. For example, UV irradiation is widely used in materials science, chemistry, biology, and many other areas to change the bulk and surface properties of various materials, substrates, and interfaces.[1−6] For almost a century, UV treatments have been among the most effective and straightforward methods of disinfection with the cleaning and/or deactivating microorganisms through the irradiation of surfaces.[7−10] UV light exposure is also a primary tool in food, water,[11−13] and air purification.[14] In addition to surface sterilization, UV light treatments have been used to control synthetic chemical reactions. UV light alters the surface chemistry of many materials to form catalytic sites[15,16] or oxides.[17−19] Furthermore, UV light is the reaction initiator in many polymer cross-linking processes where it triggers the formation of additional bonds between polymeric chains.[20−23] In these applications, UV irradiation is a practical methodology with many advantages including its noninvasive delivery, its applicable to broad range of materials, the low cost of UV systems, and the speed of its application.

Certain classes of materials such as semiconductors undergo a number of changes after exposure to UV light. More specifically, UV irradiation induces a free charge carriers in which (1) there is an accumulation of surface charge and (2) it may lead to changes in the bulk material, such as increased electrical conductivity.[24,25] The importance of this phenomena, the reasons why they arise, and possible influence of doping levels of substrate materials used were studied in previous work of our research group.[26] While the effects of UV irradiation on different semiconductor materials are used in many applications, little work has been done to examine how UV light can be applied to biointerfaces to alter interfacial properties and control the behavior of microorganisms without killing them. In our prior work we have demonstrated that the properties of wide bandgap materials in conjunction with UV light can play a part in biointerfaces with mammalian cells.[26−28] We seek to

Received: May 31, 2019
Accepted: July 30, 2019
Published: July 30, 2019

DOI: 10.1021/acsaelm.9b00347
ACS Appl. Electron. Mater. 2019, 1, 1641−1652

Scheme 1. (A) Generation of Reactive Oxygen Species after a Material Is Exposed to UV Light in the Presence of Water; (B) Change in the Interface Characteristic of GaN after Exposure to UV without Immersion in Water; and (C) Representation of Our Biointerface Experiments[a]

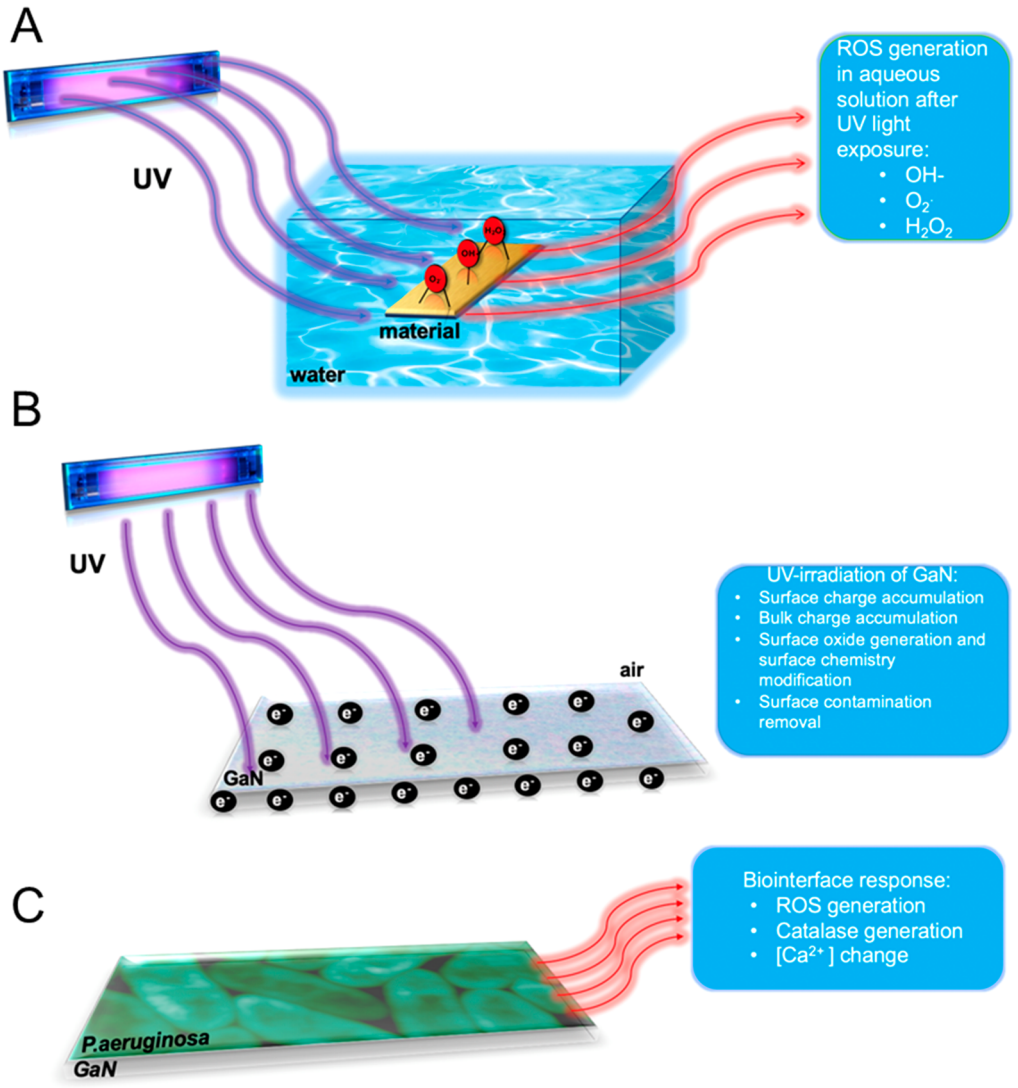

[a]*P. aeruginosa* is placed in contact with GaN surfaces that have either been exposed to UV light or not. One observes changes in *P. aeruginosa* behavior as a result of contact only with the GaN that has been treated with UV light. The bacteria are never directly exposed to the light.

extent the utility of wide bandgap materials that incorporate living microorganisms and show that they can serve as a versatile bioelectronic interface.[29]

In this study, we used GaN semiconductor thin films with doped with Si to obtain different carrier concentrations: 1×10^{18} and 2×10^{19} cm^{-3} (medium and high doping concentration, respectively). The surface charge of the films was changed by exposure to UV light, and the altered interfaces were employed to modulate the behavior of *Pseudomonas aeruginosa* (Scheme 1). We aim to use UV light to alter the properties of semiconductor interfaces but not for the purposes of developing an antibacterial material. In our prior work, we have shown that *P. aeruginosa* grows and remains healthy on GaN.[30] During the entire study we never exposed the bacteria directly to UV light, in contrast to what other researchers have done to explore antibacterial materials.

Pseudomonas aeruginosa has a high resistance to antibiotics and can utilize various mutation mechanisms as a reaction to alterations in the surrounding environment. All these factors make *P. aeruginosa* an excellent candidate for these studies due to its relevance in biomedical research and its ability to quickly adapt to changes in external conditions.[31−34] We aim to show in this work that UV-treated GaN surfaces can serve as programmable functional interfaces that contain living bacteria.[35] With this in mind we show that changes in semiconductor surface properties can be programmed to change the *P. aeruginosa* behavior without killing it. To understand the behavior of GaN−*P. aeruginosa* biointerfaces, surface characterization of the materials was performed along with biological assay studies. Chemical composition, topography, and surface charge of the GaN samples were quantified by X-ray photoelectron spectroscopy (XPS), atomic force microscopy (AFM), Kelvin probe force measurements (KPFM), and contact angle (CA) measurements. Reactive oxygen species (ROS) assay, catalase activity assay, and calcium concentration assay tests were utilized to determine the behavior of *P. aeruginosa* films under different interfacial conditions. We monitored Ga release into the aqueous

DOI: 10.1021/acsaelm.9b00347
ACS Appl. Electron. Mater. 2019, 1, 1641−1652

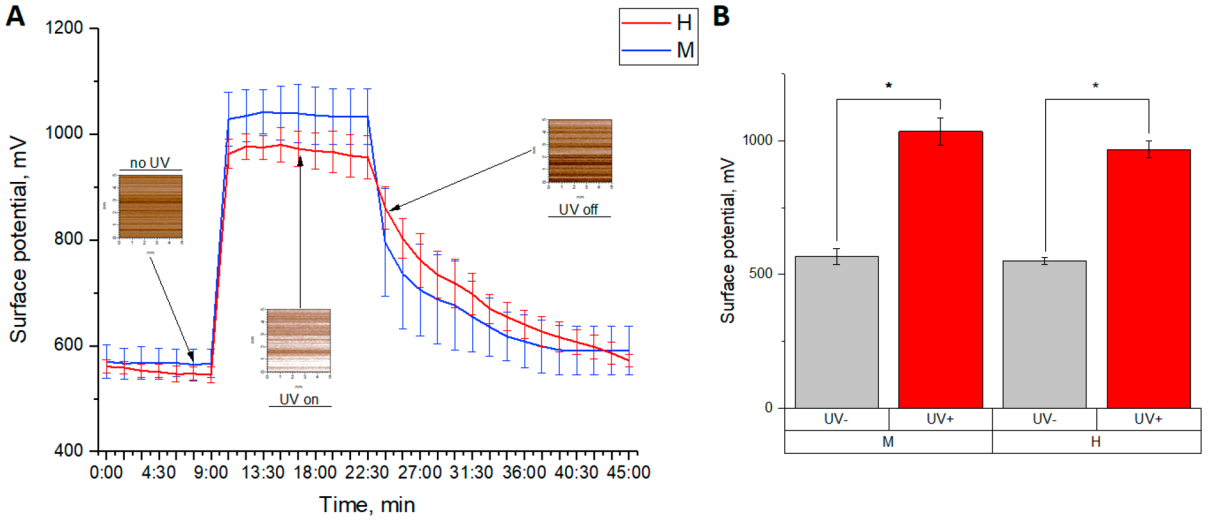

Figure 1. (A) KPFM time-dependent measurements of GaN samples under UV irradiation along with (B) mean surface potential values evaluated by KPFM of nonexposed and exposed to the UV light GaN^{m} and GaN^{h} samples.

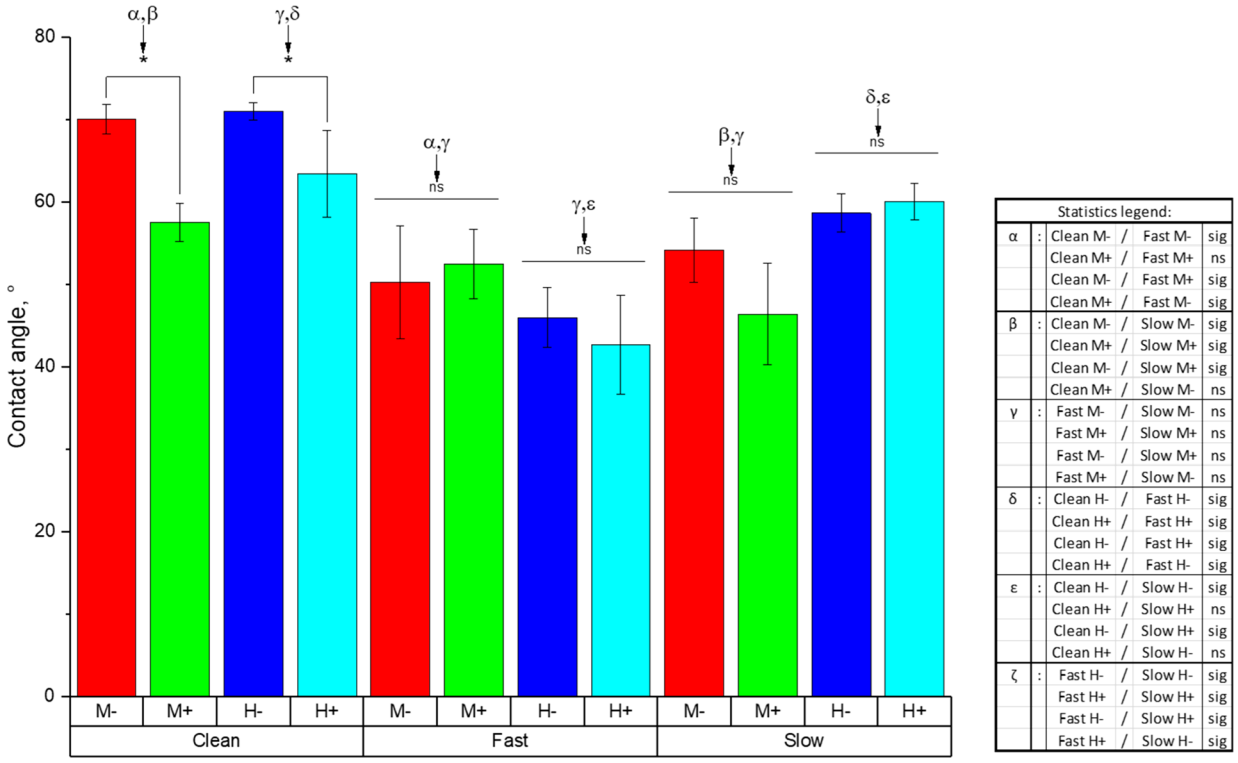

Figure 2. Changes in water contact angles of clean and modified GaN surfaces. M and H indicate medium and high doping respectively, whereas − and + are used to indicate no exposure and exposure to UV light, respectively.

solutions using inductively coupled plasma mass spectrometry (ICP-MS). In this work we demonstrated that the quantitative and qualitative changes to the *P. aeruginosa* films are directly related to changes in the GaN materials' interfacial properties in a UV-activation-dependent manner, which supports the notion that GaN films can be the "control unit" of functional biointerfaces.

2. RESULTS AND DISCUSSION

Substrate Surface Characterization. We began this work by hypothesizing that the accumulation of charge on the surface of inorganic samples is a significant way to manipulate the response of biological system formed on a GaN surface. However, prior work has shown that bacterial film formation and behavior can be manipulated by other interfacial characteristics such as surface roughness.[36−38] In our own work with the same materials we have demonstrated that surface roughness can be an important factor in cell adhesion.[39,40] Therefore, we assess the surface characteristics of GaN samples with two different doping concentrations ($GaN^{m(edium)}$ and $GaN^{h(igh)}$) that were either treated or not treated with UV light. We characterized the roughness of clean GaN samples using AFM topography imaging. The roughness was 0.962 nm with a standard deviation (SD) of 0.514 nm for

DOI: 10.1021/acsaelm.9b00347
ACS Appl. Electron. Mater. 2019, 1, 1641−1652

GaN^m and 0.731 nm (SD 0.250 nm) for GaN^h. To check a possible effect of the illumination with UV light, we collected scans right after the UV treatment. Root mean-square (rms) roughness values were 0.903 nm (SD 0.419 nm) for GaN^m and 0.821 nm (SD 0.302 nm) for GaN^h samples. Statistical analysis supports the conclusion that UV light irradiation of all of the types of GaN samples does not significantly affect their roughness.

The change in surface charge of GaN^m and GaN^h samples was quantified by using KPFM (Figure 1). Figure 1a shows how surface charge changes with time under different external conditions (no UV light, UV light is on, and finally, UV light is off). One observes a slow decay of the charge after the UV irradiation was stopped. Figure 1b represents the values of surface potential of GaN^m and GaN^h substrates before and right after UV irradiation. The mean values are the following: 567.04 and 1035.38 mV (438.34 mV increase) for GaN^m; 551.60 and 968.35 mV (416.75 mV increase) for GaN^h samples. On the basis of the statistical analysis, we consistently detected a significant increase upon UV illumination of all GaN samples. GaN^h samples have slightly higher surface potential after the removal of the UV light exposure and a slower decay rate, which means that the charge decay time is longer than one for GaN^m samples. However, GaN^h samples have lower surface potential for initial and UV-irradiated conditions (Figure 1). Thus, the amount of doping does not result in a significant difference in surface potential change and plays a larger role when we move deeper from the surface, which correlates with theoretical and experimental observations of these semiconducting materials.[41,42] Generally, semiconductors of various types (and GaN as one of them) possess a significant amount of charge carriers concentrated in a close proximity to the surface, which tend to play a role in the bulk properties.[28,39] The above-mentioned carriers are responsible for occupying surface energy states, whose configurations are defined by the chemical composition and polarity of the material deposited. Furthermore, the finite number of allowed surface energy states explains the fact that the difference in surface potential between GaN samples of different doping level is insignificant.

UV light has been routinely used to clean different types of surfaces[43,44] and change the hydrophobicity of materials.[43,45,46] We carefully evaluated changes of contact angle (CA) of prepared GaN samples under the following conditions: (1) clean−clean GaN^m and GaN^h samples; (2) fast-GaN samples, which are GaN substrates with a *P. aeruginosa* biofilm which is removed by vortexing and subsequently removed from the DPBS solution; and (3) slow-GaN samples, which are GaN substrates with a *P. aeruginosa* biofilm, which is removed by vortexing and returned to the DPBS solution overnight. UV treatment was done by the exposure of clean equilibrated samples to the UV light source for 1 h. The baseline data of the clean GaN samples allowed us to evaluate the changes to the surface properties of the GaN materials caused by the formation of *P. aeruginosa* biofilms and various alterations in external conditions. Additional details regarding sample preparation procedures are provided in the Experimental Section. Figure 2 summarizes all CA results for all conditions before and after exposure to the UV light. For the clean samples we observed a significant difference in CA for both GaN^m and GaN^h substrates between UV-treated and non-treated samples. GaN^m samples had CA of 70.08° for UV− and 57.58° for UV+ samples; GaN^h samples had CA values of 71.05° and 63.45° for UV− and UV+, respectively. For both fast and slow sets of samples, GaN^m and GaN^h did not show a significant difference between clean UV-exposed and UV-irradiated samples. The difference between fast and slow sets of GaN samples was not significant, which suggests that the changes to the substrate's hydrophobicity due to *P. aeruginosa* biofilm formation are rapid and irreversible. However, there were significant differences among clean, fast, and slow treated sample sets of both GaN^m and GaN^h that were not exposed to the UV light. Detailed information regarding interactions between different conditions and material combinations can be seen in statistics legend. Basic statistical comparison is performed on UV-exposed and nonexposed materials of the same condition: significant difference is shown with an asterisk (∗) and nonsignificant difference is expressed as (ns). Here and further in the text, Greek alphabet letters are used to mark statistical interactions between various materials and conditions. For example, alpha (α) distinguishes the interactions between clean and fast gan samples. In the legend, one can see all interactions tested for α: direct statistical comparison between fast and clean UV-illuminated samples along with indirect UV-positive/UV-negative fast and clean samples. Other statistical interactions are presented in the same manner and can be observed following the same logic of reading the statistical legend insets in pictures of this article. Here in Figure 2, the differences in the results among the three conditions (clean, fast, and slow) can be explained by the formation of oxides on the surface of samples upon exposure of liquid solutions for fast- and slow-treated samples. Furthermore, an effect of UV irradiation diminishes with time, and in the case of fast and especially slow conditions it completely fades away. As a result, one records no significant difference between UV− and UV+ samples, as it shown on the graph. However, all the gathered measurements help us to better understand how different conditions can affect the hydrophobicity of GaN^m and GaN^h samples used in our experiments.

We subsequently quantified the elemental composition of the prepared GaN^m and GaN^h samples by XPS. We initially analyzed survey scans allowing us to access the chemical composition of a surface along with possible change caused by different external conditions. The XPS scans of the clean, fast, and slow GaN^m and GaN^h samples are in Figure 3. All the numerical values of chemical composition contributions can be found in the Supporting Information. The total chemical composition of clean GaN samples has four major contributors: Ga, N, C, and O (Figure 3a). Clean GaN^m samples express the following changes under UV irradiation: Ga shows a 1.46% decrease, N shows a 3.98% decrease, C shows a 38.77% increase, and, importantly, O shows a 20.46% increase. We observed similar results for clean GaN^h: Ga contribution decreased by 3.69%, N increased by 3.07%, C shows a 27.29% increase, and O increased by 8.42% for UV-irradiated samples. There was no significant change in all contributing chemical elements for both GaN^m and GaN^h substrates upon exposure to the UV light. XPS analyses of fast and slow treated GaN substrates express two additional components, Na and Cl, which are presented in the DPBS solutions. Fast-treated UV+ GaN^m samples expressed the following changes to their chemical composition when compared to nonirradiated samples: Ga composition decreased by 2.33%, N composition decreased by 1.14%, C composition increased by 32.82%, Na content increased by 49.69%, and the Cl content increased by 62.65%. Fast GaN^h samples were characterized with the

DOI: 10.1021/acsaelm.9b00347
ACS Appl. Electron. Mater. 2019, 1, 1641−1652

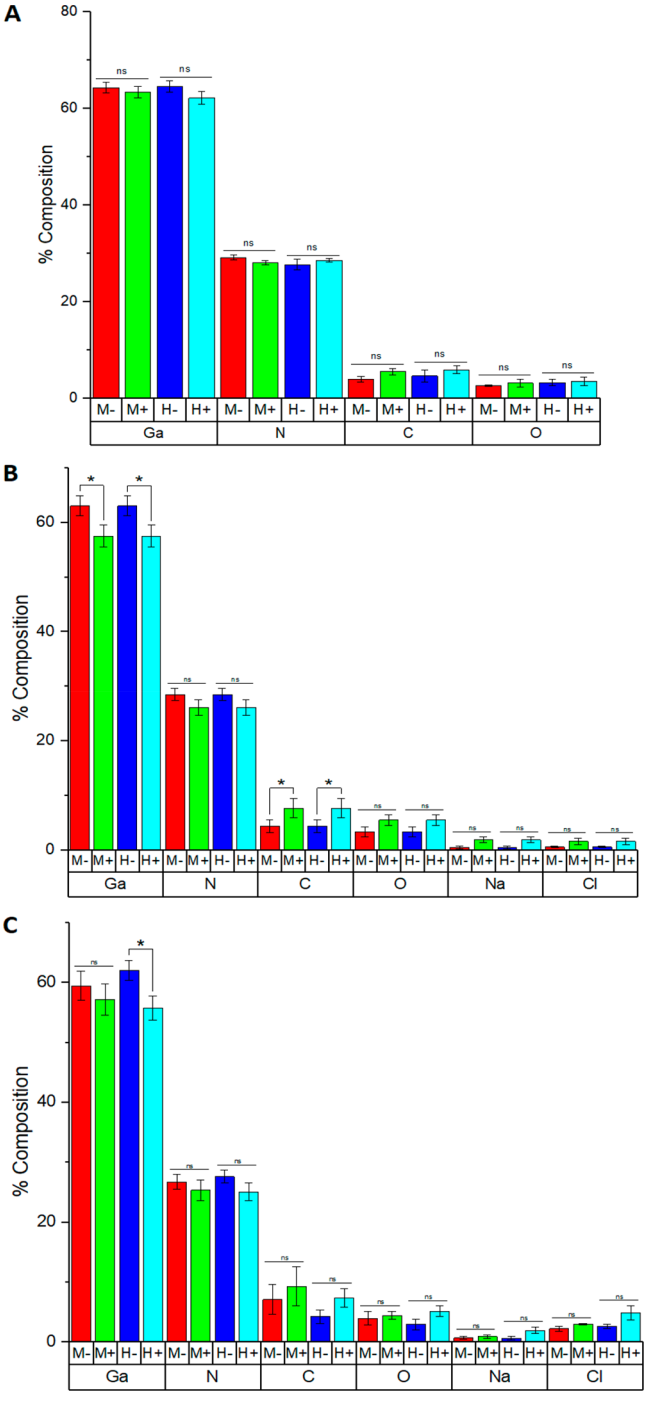

Figure 3. Chemical compositions of (A) clean GaN surfaces, (B) fast-treated GaN surfaces, and (C) slow-treated GaN surfaces obtained by processing and analyzing of XPS survey scans. The data are collected on GaN^m and GaN^h samples both equilibrated in the dark (−) and exposed to the UV light (+).

following changes to their chemical composition after exposure to the UV light: Ga composition decreased by 8.74%, N showed a decrease of 8.25%, C showed a 76.07% increase, the O content increased by 66.36%, the Na concentration increased by almost 3 times, and Cl almost doubled its amount. Only Ga and C express a significant statistical difference upon exposure to the UV light for both GaN^m and GaN^h samples (Figure 3b). The increased carbon contamination appeared to be caused by contact with *P. aeruginosa* biofilm and was greater in the UV-treated samples. XPS analysis of slow-treated GaN^m and GaN^h samples showed similar changes to their chemical composition as fast-treated samples (Figure 3c). XPS analysis of slow-treated GaN^m change between UV− and UV+ compositions is the following: Ga content decreases by 3.82%, N content decreases by 5.07%, C content increases by 31.36%, O content increases by 11.59%, Na shows a 29.53% increase, and Cl has a 34.39% increase. Slow-treated GaN^h samples are characterized with 10.14% decrease in Ga content, a 9.21% decrease in N content, a 74.08% increase in C content, and a 74.72% increase in O content (Figure 3c). Furthermore, we find that the Na concentration doubles and Cl increased by 84.25% on slow-treated GaN^m surfaces after UV+ activation. Between GaN^m and GaN^h substrates after UV irradiation, the only significant difference observed was the change in Ga content where GaN^h samples showed a significant difference after UV irradiation. Comparing fast- and long-treated GaN samples, the increase in Cl deposition correlated to the increase incubation in DPBS buffer solution. These results confirm that UV irradiation of the GaN surfaces and the presence of a *P. aeruginosa* biofilm alter the chemical composition of the GaN surface in a rapid manner.

Upon exposure to liquid solutions, one needs to consider the formation of oxide species because they can ultimately lead to dissolution of metal species in solution, which have been shown to change the survival of bacteria.[47,48] Important surface changes can be tracked through the presence of variable types of oxygen and carbon species. Thus, we analyzed the narrow XPS scans of O 1s and C 1s spectra for clean, fast-treated, and slow-treated GaN samples (Figure 4). The O 1s spectrum contains three components: metal oxide (Ga_2O_3), hydroxyl groups (OH), and water with carbon contamination (Figure 4a). Overall, fast- and slow-treated GaN^m and GaN^h samples show a decreasing trend of metal oxide content and an increase in OH group contribution. The amount of water and carbon contamination is slightly larger for both fast- and slow-treated GaN samples when compared to clean GaN samples. There was no significant difference in the content of O species between UV− and UV+ samples for both GaN^m and GaN^h samples (Figure 4). The C 1s spectrum consists of three major contributors: C−C, C−O−C, and O−C═O bonds (Figure 4b). Both fast- and slow-treated samples show a significant decrease from clean GaN samples in the presence of C−C bonds but an overall increase in both C−O−C and O−C═O bonds (Figure 4b). The difference between fast and slow GaN samples is not statistically significant. We observe no significant difference in the C1 spectra of GaN^m and GaN^h treated either way after UV treatment. Another indicator of a change in chemical properties can be accessed through Ga 2p spectra deconvolution. All samples examined had overlapping Ga $2p_{1/2}$(element) and Ga $2p_{1/2}$(native oxide) components, and therefore we monitored the potential changes to the oxidative state of Ga through the Ga 2p peak spectra. We observed a small but significant shift toward lower binding energies in fast- and slow-treated GaN samples when compared to clean GaN, both medium and high doped. However, we did not observe any significant differences in the Ga 2p peak position after UV irradiation in any sample.

There is a possibility that the increased amount of oxide on the surface of GaN samples can facilitate the release of Ga in solution. We measured the dissociation of Ga ions from the GaN surfaces into aqueous solutions by ICP-MS. In these

DOI: 10.1021/acsaelm.9b00347
ACS Appl. Electron. Mater. 2019, 1, 1641−1652

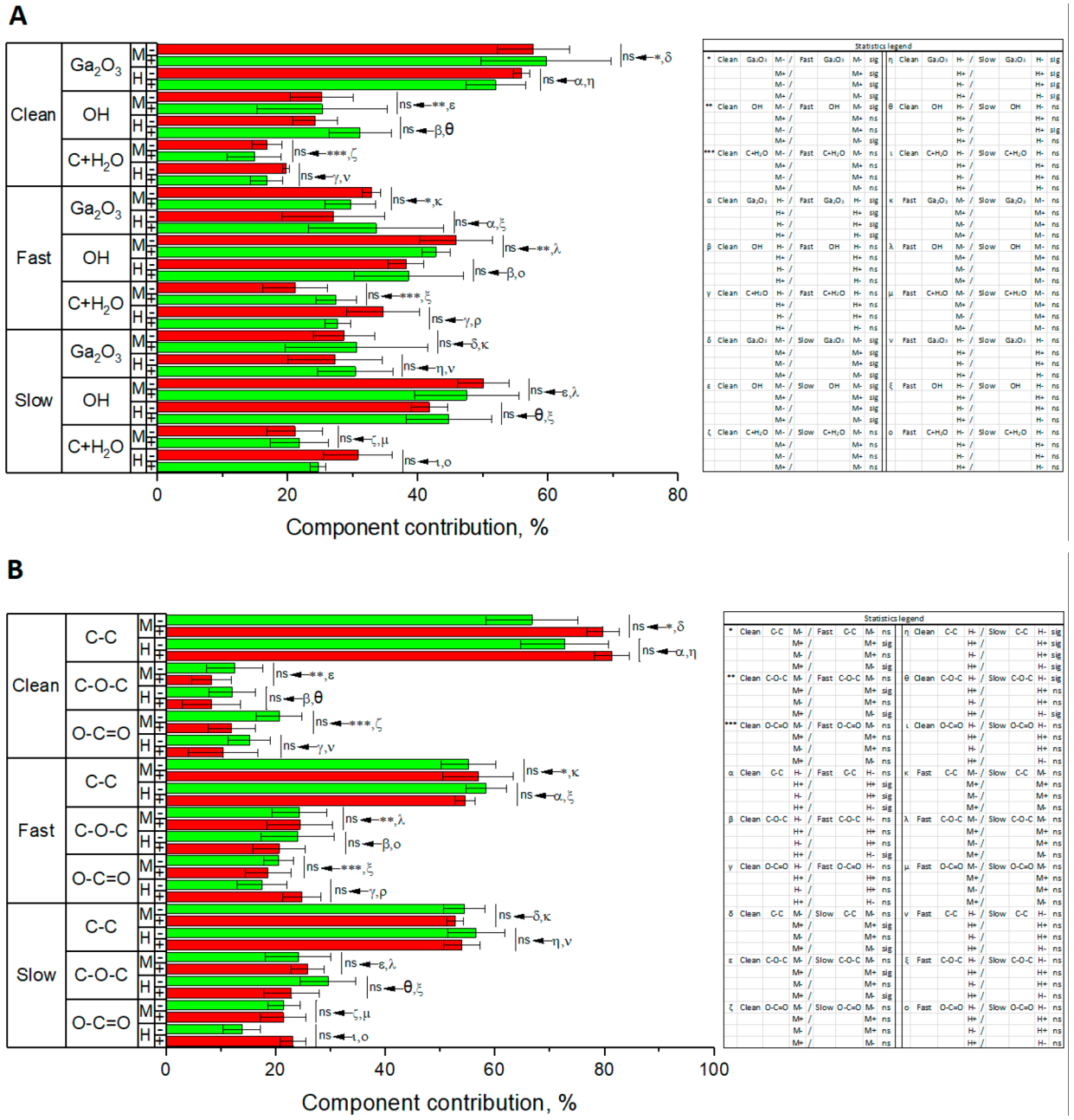

Figure 4. XPS analysis of the high-resolution data in the following regions: (A) O 1s and (B) C 1s regions for clean, fast-treated, and slow-treated samples. GaN^m and GaN^h samples were measured as equilibrated (−) and after exposure to the UV light (+). Statistical analysis interactions are available in the legends. High-resolution pictures can be found in the Supporting Information.

experiments we tested the solutions incubated with both GaN^m and GaN^h and treated under all conditions, UV+/− and long/slow (Figure 5). We measured Ga by ICP-MS after all interfacial conditions, although statistically there was no significant difference among any all of the condition treatments (clean, fast, and slow), doping concentration, or in UV irradiation vs no UV irradiation (Supporting Information). Clean GaN samples exhibited Ga concentrations in the range 19.9−27.7 μg/L. For fast- and slow-treated GaN samples, the range increased to 22.1−69.1 and 27.3−58.7 μg/L, respectively. We also tested the blank, DPBS, and peroxide solutions for the presence of Ga traces, and all samples were below the ICP-MS detection limits. We conclude that the amounts of Ga present in the solution due to dissociation from the GaN are not responsible for differences *P. aeruginosa* behavior. These results also support the notion that if there are changes in the *P. aeruginosa* behavior after exposure to the variably treated GaN materials, they are interface dependent rather than being mediated by variable amounts of dissociated metal ions in solution.

Biointerface Response Tests. There are a variety of established ways of monitoring the biological response to environmental changes during bacterial growth and biofilm development.[49−52] The changes in oxide content of the fast- and slow-treated GaN surfaces that had been subjected to *P. aeruginosa* biofilms suggested that the presence of this living layer was responsible for these chemical changes to the surface. A significant response component to many biological systems

DOI: 10.1021/acsaelm.9b00347
ACS Appl. Electron. Mater. 2019, 1, 1641−1652

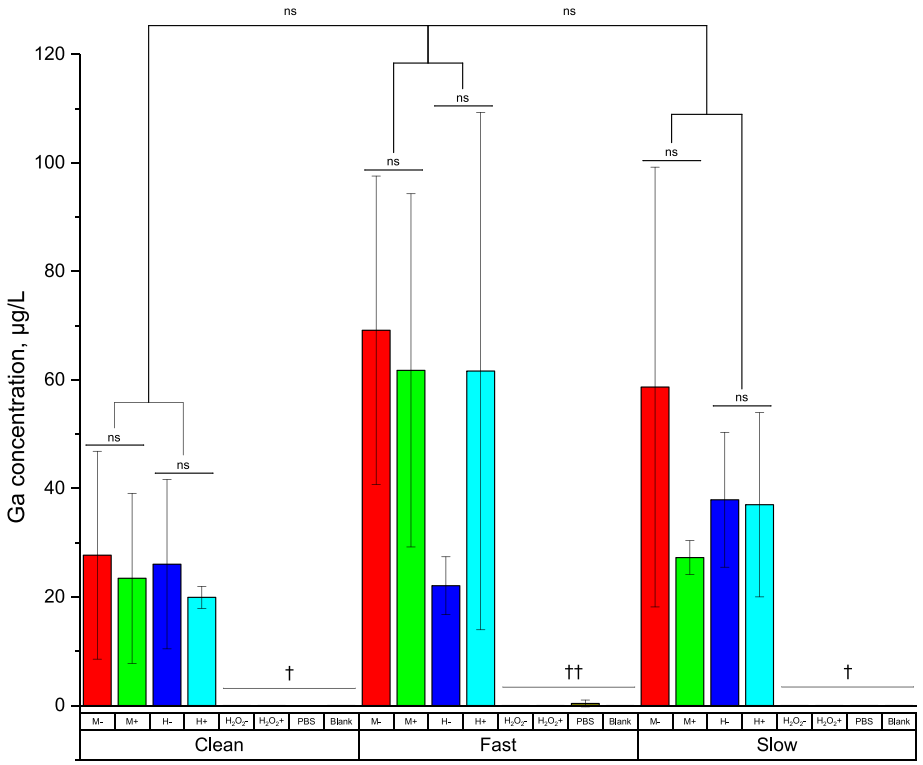

Figure 5. ICP-MS data for all solutions used in the ROS dye experiments. Clean, fast, and slow sets of samples were evaluated for Ga leakage. UV− and UV+ samples represent equilibrated and UV-irradiated samples. Note: † = amount of Ga was below detection limits (<1.0 ug/L); †† = for all solutions but DPBS amounts of Ga were below detection limits. For DPBS, tests report the value of 1.1 μg/L, which is still considered to be insignificant.

including bacterial biofilm formation is the presence of free radical oxygen species (ROS). To determine whether there is an increase in ROS species on these GaN surfaces, we utilized a dye (2′,7′-dichlorofluorescein diacetate) sensitive to multiple types of reactive oxygen species (ROS). They include hydrogen peroxide (H_2O_2), hydroxyl radical ($^{\bullet}OH$), superoxide radical ($^{\bullet}O_2^-$), and singlet oxygen ($^1O_2$) and can be produced during internal cellular response to alterations of external conditions.[53−55] The same as in previous characterization sections, we examined clean, fast-treated, and slow-treated GaN samples. The exposure to UV irradiation was always for 1 h prior to any other experiments. Compiled results of ROS dye tests are represented in Figure 6. For all conditions, hydrogen peroxide was used as a positive control to establish the validity of the assay. Clean dye solution is denoted as blank. Initially we determined the amount of ROS species on GaN surfaces before and after UV irradiation (Figure 6a). We find that there is no significant difference for both GaN^m and GaN^h samples when compared to the blank. Furthermore, UV light causes no significant difference in ROS production when one compares UV-treated and nontreated samples. However, incubation of both GaN^m and GaN^h surfaces with *P. aeruginosa* resulted in elevated levels of ROS generation (Figure 6b,c). In both the fast- and slow-treated GaN samples the amount of ROS generated by *P. aeruginosa* cells washed from GaN^m and GaN^h samples is significantly greater than blank and obviously greater than the amount from clean, untreated samples. There is no significant change in the signal level for UV− and UV+ samples. Control experiments show that the DPBS buffer alone generated no autofluorescence signal, confirming that it was the presence of a *P. aeruginosa* biofilm in contact with a GaN substrate that generated the high levels of ROS. Slow-treated GaN samples produced similar results as the fast-treated samples, although the total signal is lower than that found on fast-treated samples (Figure 6c). As with the fast-treated samples, we observed no significant change in ROS generated florescence after UV irradiation of the GaN. However, the overall amount of signal from GaN is lower than in the case of fast samples. To comment on this fact, one should notice the difference in the signal produced by H_2O_2, blank, and DPBS. Blank and DPBS levels still stay at the comparable levels, thus indicating slow degradation and overall stability of dye solution with time. Hydrogen peroxide increases the level of signal in the case of slow samples, showing that the dye degrades after prolonged exposure to ROS as witnessed by the signal increase. These results suggest that prolonged exposure of the *P. aeruginosa* biofilm allows the bacteria to adjust to the surface conditions by removing or lowering the increased ROS species. Furthermore, this effect is independent of doping level, and that the amount of doping in GaN samples does not play a significant role in this response of the *P. aeruginosa* biosystem studied.

As we showed above, the GaN substrate results in a bacterial response, specifically the increased production of ROS. To determine whether *P. aeruginosa* cell behavior is altered by Ga in the absence of interface substrate, we tested whether various concentrations of ionic Ga altered bacterial ROS production. We generated Ga ion in solution using commercially available salt gallium nitrate ($Ga(NO_3)_3$). We used several concentrations (1, 0.5, and 0.25 μg/L), and the negative control (no salt) was just *P. aeruginosa* cell/dye suspension on an insert glass coverslip substrate. The gallium nitrate solutions were used in two different ways: (1) as droplets that were put on the

DOI: 10.1021/acsaelm.9b00347
ACS Appl. Electron. Mater. 2019, 1, 1641−1652

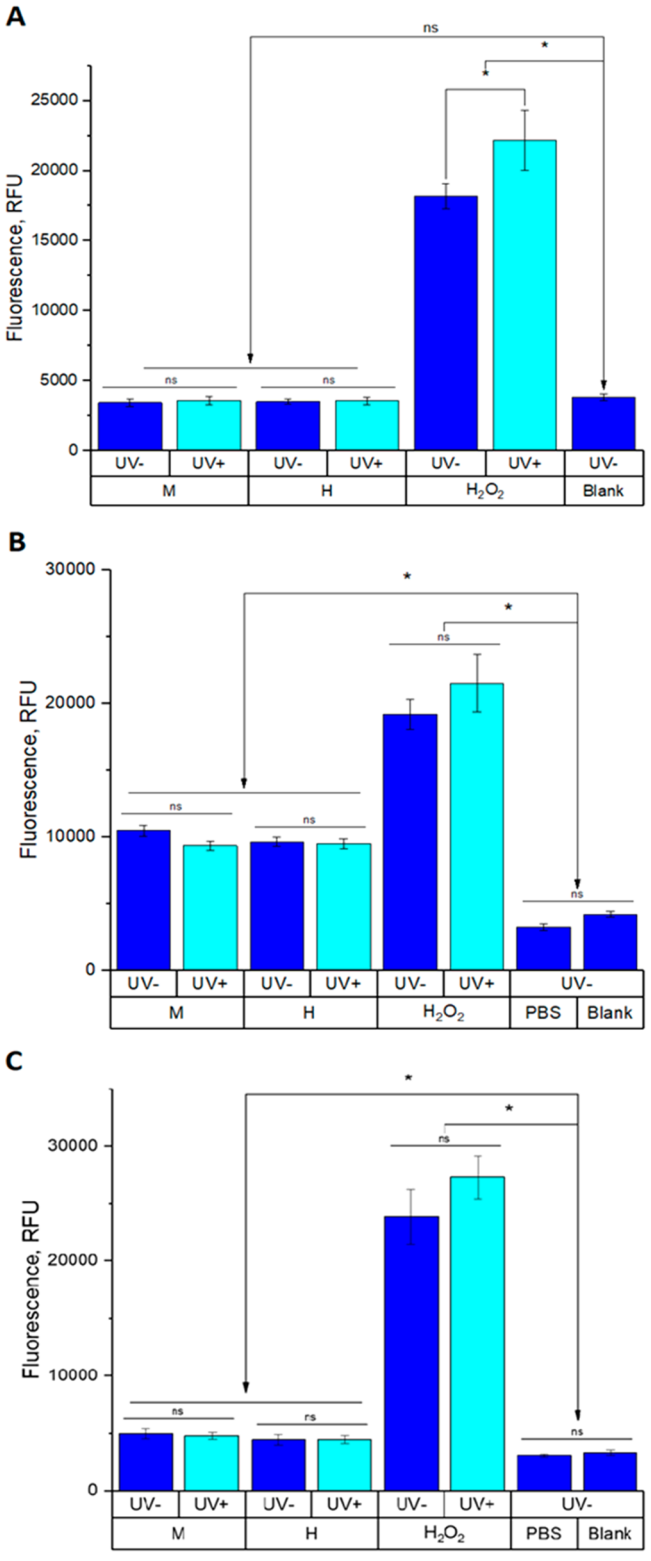

Figure 6. ROS studies of *P. aeruginosa* on GaN for (A) clean, (B) fast-treated, and (C) slow-treated samples. GaN^m, GaN^h, and hydrogen peroxide were UV-irradiated to see the change in the amount of ROS from nontreated samples. DPBS and blank serve as important reference points introducing the baseline of the fluorescence signal.

surface of agar with *P. aeruginosa* cells before biofilm formation step and (2) as solutions where the initial amount of *P. aeruginosa* cells was suspended and used to form the biofilm. The two different modes of biofilm-initiating *P. aeruginosa* bacteria interaction allowed us to test two parameters. In the droplet technique only, the *P. aeruginosa* cells contacted the substrate (i.e., glass coverslip) experienced the Ga ions, while in the solution technique, all bacteria in the Petri dish were exposed to Ga ions in solutions. In the droplet assay, we observed a significant alteration in ROS production for all Ga solutions with *P. aeruginosa* cells when compared to blank (Figure 7a, Supporting Information). Also, no-salt, 0.25 μg/L, and 1 μg/L express the significant difference in signal levels as well. In the solution assay, we observed a linear dependence of production ROS with gallium nitrate concentrations (Figure 7b). All tested solutions possess signals significantly higher levels of ROS production than blank; 0.5 and 1 μg/L solutions produce signals that were significantly greater than no-salt *P. aeruginosa* cell solution. The results summarized in Figure 7 support the notion that the presence of an interface can suppress the effect of Ga ions in solution and impede the production of ROS even in the presence of ample amount of metal ions in solution.

We also examined the change of intercellular calcium (Ca^{2+}) concentrations as a possible bacterial behavior indicator related to stress responses necessary to maintain homeostasis.[56,57] A Fluo-4 direct Ca assay monitored changes after each experimental variation. We recorded Fluo-4 fluorescent levels (Figure 8) immediately after incubation of *P. aeruginosa* with GaN^m and GaN^h substrates (both UV− and UV+). We observed a significant increase in Fluo-4 fluorescence on GaN substrates that been UV-irradiated when compared to nonirradiated GaN controls. The level of doping changes the magnitude of the response. Along with the KPFM data, obtained experimental data allow to conclude that the intracellular calcium alterations in *P. aeruginosa* biolayers are related to surface potential changes in GaN samples.

Because we observed a significant increase in ROS production by *P. aeruginosa* biofilms in the presence of Ga, we investigated whether part of this response included expression of the oxidative stress enzyme, catalase. Catalase is an enzyme found in most organisms that specifically decomposes hydrogen peroxide to water and oxygenation serves as an indicating factor of an oxidative stress response.[58,59] Particularly, catalase concentration correlates with the amount of ROS species in the cell.[60] Using a colorimetric Catalase activity assay, we tested *P. aeruginosa* biofilms formed on GaN^m and GaN^h samples that either had been irradiated with UV light or not (Figure 9). We observe that both UV-irradiated GaN^m and GaN^h sets have a significant increase in catalase activity when compared to the control, nonirradiated samples. These results correlate with the observed increase in intracellular calcium. Furthermore, because the results are collected immediately after contact with variably treated GaN, one can conclude that the change in surface potential is the initial trigger of *P. aeruginosa* biofilm response.

3. CONCLUSIONS

In summary, we formed and analyzed GaN−*Pseudomonas aeruginosa* biofilms on variably doped semiconductor surfaces. We detected *P. aeruginosa* responses as a result of changes in interfacial conditions (i.e., change in surface potential of the semiconductor). UV irradiation of GaN samples of different doping concentration levels can not only trigger surface chemistry changes but also alter the behavior of the *P. aeruginosa* within the biofilm. Furthermore, the bioassays

DOI: 10.1021/acsaelm.9b00347
ACS Appl. Electron. Mater. 2019, 1, 1641−1652

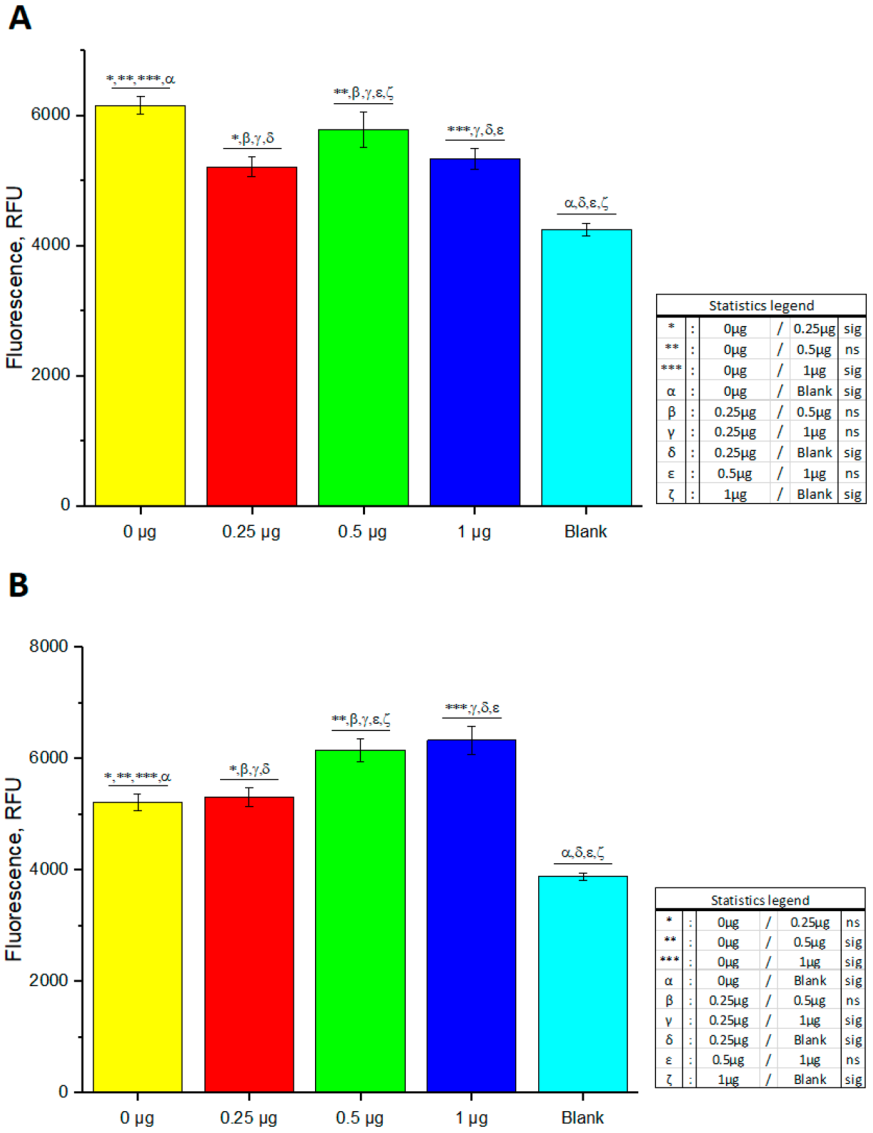

Figure 7. ROS studies of $Ga(NO_3)_3$ salt for (A) droplet and (B) solution techniques applied to *P. aeruginosa* cells initializing the biofilm formation. 0 μg represents cells not affected by salt. Blank expresses the baseline fluorescence signal. Statistical analysis interactions are available in the legends.

performed for Ca^{2+} and catalase showed that the magnitudes of the *P. aeruginosa* changes are dependent on the GaN doping. The results of this work can be used to tune the function of biointerfaces that incorporate living microorganisms.

4. EXPERIMENTAL SECTION

Materials and Supplies. Biofilm preparation materials such as the culture, media ingredients, and other specifics are detailed in prior studies.[30] All supplies necessary for new experiments were used as it stated in the manufacturer's documentation: HyClone DDPBS (Dubelcco's phosphate-buffered saline)/modified, 500 mL (Cat. SH30028.02), ordered from GE Healthcare Life Sciences; DMSO (dimethyl sulfoxide), 250 mL (ref 25-950-CQC), ordered from Corning Mediatech; Corning 96-well clear polystyrene microplate (Mfr.# Corning3358), ordered from Sigma-Aldrich; 2′,7′-dichloro-fluorescein diacetate (crystalline), 250 mg (CAS 76-54-0), ordered from Sigma-Aldrich; DetectX catalase colorimetric activity kit (Cat. K033-H1), ordered from Arbor Assays; hydrogen peroxide (30%), 500 mL (Cat. BP2633500), ordered from Fisher Scientific; ASYELEC.01-R2 AFM probes with conductive Ti/Ir coating, frequency f = 75 kHz and spring constant $k = 2.8 \frac{N}{m}$, ordered from Oxford Instruments; gallium(III) nitrate hydrate (crystalline), 25 g (Lot MKCC1844), ordered from Sigma-Aldrich; UVP mini UV lamp (Cat. U-2221-13), purchased from Analytik Jena. GaN with Ga-polar GaN (medium) and (high) types was grown as previously reported in our laboratories.[61−63]

Biofilm Sample Preparation. All procedures associated with substrate preparation are described in Foster et al.,[64] and the biofilm growth and UV treatment are also adapted from prior work.[30] Briefly, droplets with *P. aeruginosa* solutions were spread on the agar, and then prepared GaN samples were transferred into these culture dishes. Further incubation lasted for 8 h, and as a result, a bacteria layer of required thickness was grown on the surface of GaN samples. GaN UV+ samples were treated as stated above before putting them on the agar plates with bacteria. UV+ hydrogen peroxide solutions were irradiated for 1 h in uncovered wells, thus being directly exposed to the UV light.

$Ga(NO_3)_3$ Samples Preparation. $Ga(NO_3)_3$ salt solutions (droplets) were prepared by dissolving crystalline $Ga(NO_3)_3$ in deionized water to obtain the desired (1, 0.5, 0.25, and 0 μg/L—no salt added) concentrations. By use of the biofilm sample preparation steps, a droplet with *P. aeruginosa* culture was spread on the surface of the prepared agar plate. Droplets (25 μL) of $Ga(NO_3)_3$ were put onto the surface of the agar and then covered with sterile glass coverslips. Samples then were incubated at a temperature of 37 °C for 8 h.

DOI: 10.1021/acsaelm.9b00347
ACS Appl. Electron. Mater. 2019, 1, 1641−1652

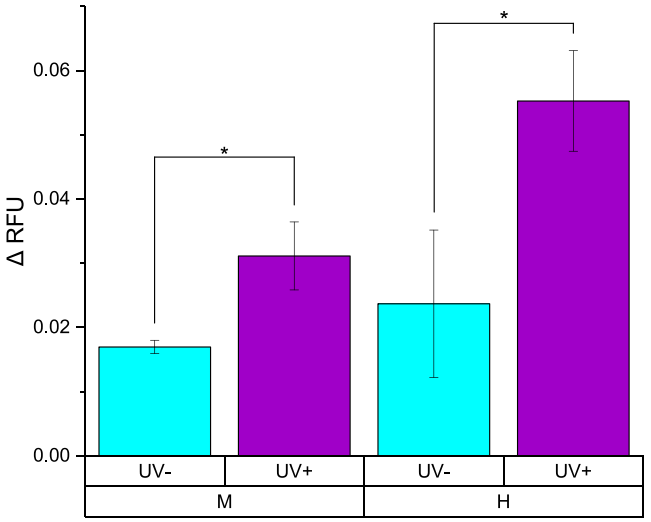

Figure 8. Results of Fluo-4 direct calcium assay tests. Fluorescence was measured for *P. aeruginosa* cells on the surface of GaN^m and GaN^h samples before and after exposure to the UV light.

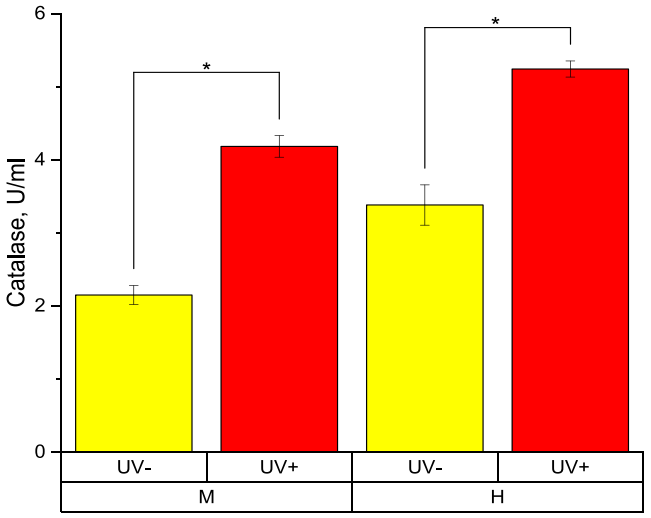

Figure 9. DetectX catalase colorimetric activity kit data. *P. aeruginosa* biofilm cell response was evaluated for GaN^m and GaN^h samples before and after UV irradiation.

$Ga(NO_3)_3$ salt solutions (solution) were prepared by dissolving crystalline $Ga(NO_3)_3$ in deionized water to obtain desired (1, 0.5, 0.25, and 0 μg/L—no salt added) concentrations. A *P. aeruginosa* pellet from biofilm preparation steps was dissolved in obtained $Ga(NO_3)_3$. Droplets (45 μL) of the prepared *P. aeruginosa*-$Ga(NO_3)_3$ solutions were spread on the agar surface and covered with transferred coverslips. Further incubation required 8 h at a temperature of 37 °C.

ROS Assay Test. 2′,7′-Dichlorofluorescein diacetate solution was prepared according to adapted protocols available.[65] The 1 mM stock solution was prepared by dissolving 2′,7′-dichlorofluorescein diacetate in DMSO. The working dye solution of 1 μM was prepared by dissolving the stock solution in DPBS. The unused stock solution was aliquoted into a single use vial and stored at −20 °C and kept from light. Clean samples (UV− and UV+) of GaN(medium) and GaN(high) were put into working 1 μM dye solution and vortexed for 2 min. The next step involved 60 min of incubation at 37 °C. After transferring into 96-well plates, the solutions were equilibrated for ≈15 min and then read via a plate reader. Fast *P. aeruginosa* samples were prepared as follows. Samples with *P. aeruginosa* biofilms were washed by vortexing with working 1 μM dye solution for 2 min and then incubated for 60 min. Then samples were vortexed again and equilibrated, and solutions were transferred into 96-well plates and read in the plate reader. Long *P. aeruginosa* samples were prepared according to similar procedures. Samples with *P. aeruginosa* biofilms were washed by vortexing with working 1 μM dye solution for 2 min and then incubated in the dark at 37 °C for 1 h. Samples removed from an incubator, vortexed, and stored in the dark and equilibrated at room temperature for 12 h. After that, the solutions were transferred into 96-well plates and read in the plate reader. Hydrogen peroxide (0.5% solution) was used as a positive control for this dye. Blank samples (just dye solution) and clean DPBS solutions were used as a control of a fluorescence signal baseline. A Tecan GENios microplate reader performed all readings of 96-well plates (six wells for each sample in each plate). For this experiment, 492 nm excitation and a 535 nm emission filters were installed, and all analysis of raw data was performed with Origin 2018 (v. 9.5.5.409).

Catalase Activity Test. Catalase activity assay solutions and standards were prepared according to instructions provided in the manufacturer's protocol. Prepared *P. aeruginosa* samples of GaN^m and GaN^h were washed in catalase assay buffer by vortexing for 2 min. Obtained cell suspensions were transferred to 96-well plates, and then the steps from the assay protocol were completed. Ready solutions were incubated for 15 min at room temperature in the dark and then evaluated with a Tecan GENios microplate reader. The optical density was read at 570 nm. Readings (six wells for each sample in each plate) for both samples were averaged, and then curve fitting routine was performed with a help of online tool from MyAssays (available through Arbor Assays).

Calcium Assay Test. All detailed steps of the assay are available in prior work.[30] By use of the manufacturer's protocol, prepared Fluo-4 direct calcium assay was added to 96-well plates with cell suspensions (six wells for each sample in each plate) and then incubated in the dark at 37 °C for 1 h. Fluorescence measurements were performed by using Tecan GENios microplate reader with 485 nm excitation and a 535 nm emission filters installed. Origin 2018 (v. 9.5.5.409) was used for all reported analysis.

AFM Characterization. Tapping mode AFM was performed to acquire all the reported data.[30] At least three samples were prepared per each material and each condition. KPFM scans were taken with ASYELEC.01-R2 AFM probes at 1 and 2.25 Hz to create 2.5 × 2.5 μm^2, 5 × 5 μm^2, and 5 × 5 nm^2 charge distribution maps. Roughness and surface charge distribution maps were analyzed and compared across all samples in the software provided by Asylum (Asylum Research bundle) with the AFM setup.

XPS Characterization. Kratos XPS was utilized to collect all the data as reported in a number of other studies.[66−68] The following regional spectra were obtained: Ga 3d, Ga 2p, C 1s, N 1s, and O 1s. The data were analyzed via Casa XPS software package (v. 2.3.19) with adventitious carbon 1s peak value set at 284.8 eV for peak calibration purposes.

Contact Angle. As previously reported by our group,[30] the contact angles of GaN^m and GaN^h samples were measured with a ramé-hart setup (using 1.25 μL droplets of deionized water) and OnScreenProtractor Java-applet (v. 0.5) for image analysis.

ICP-MS. Solutions were submitted for analysis with a Thermo Element XR instrument. 200 μL aliquots were taken from each sample and each condition where *P. aeruginosa* samples were autoclaved before the analysis. All ICP-MS analysis was performed by the Environmental and Testing Services at NC State University. Obtained Ga concentrations were analyzed by using Origin 2017 (v. 9.4.1.354).

Statistical Analysis. For each material and each condition at least three samples were prepared and analyzed. For surface analysis tests, at least three random spots were scanned (imaged) on each sample. For assay tests, at least three 96-well plates with full set of solutions were used. Statistical analysis of the data was performed via 1-way, 2-way, and 3-way ANOVA method with Origin 2018 (v. 9.5.5.409).

DOI: 10.1021/acsaelm.9b00347
ACS Appl. Electron. Mater. 2019, 1, 1641−1652

■ ASSOCIATED CONTENT

Supporting Information

The Supporting Information is available free of charge on the ACS Publications website at DOI: 10.1021/acsaelm.9b00347.

Additional experimental details, statistical analysis, and characterization data (PDF)

■ AUTHOR INFORMATION

Corresponding Author

*E-mail: ivanisevic@ncsu.edu.

ORCID

Dennis R. LaJeunesse: 0000-0001-5049-8968

Pramod Reddy: 0000-0002-8556-1178

Albena Ivanisevic: 0000-0003-0336-1170

Notes

The authors declare no competing financial interest.

■ ACKNOWLEDGMENTS

We thank the Army Research Office (W911NF1910033) for support of this work. Partial financial support from the NSF (ECCS-1653383) is greatly appreciated.

■ REFERENCES

(1) Decker, C. Special Review The Use of Irradiation in UV Polymerization. *Polym. Int.* **1998**, *45*, 133−141.

(2) Esumi, K.; Suzuki, A.; Aihara, N.; Usui, K.; Torigoe, K. Preparation of Gold Colloids with UV Irradiation Using Dendrimers as Stabilizer. *Langmuir* **1998**, *14* (12), 3157−3159.

(3) Pandey, K. K. Study of the Effect of Photo-Irradiation on the Surface Chemistry of Wood. *Polym. Degrad. Stab.* **2005**, *90* (1), 9−20.

(4) Gassan, J Effects of Corona Discharge and UV Treatment on the Properties of Jute-Fibre Expoxy Composites. *Compos. Sci. Technol.* **2000**, *60*, 2857−2863.

(5) Oláh, A.; Hillborg, H.; Vancso, G. J. Hydrophobic Recovery of UV/Ozone Treated Poly(Dimethylsiloxane): Adhesion Studies by Contact Mechanics and Mechanism of Surface Modification. *Appl. Surf. Sci.* **2005**, *239* (3−4), 410−423.

(6) Li, M.; Neoh, K. G.; Kang, E. T.; Lau, T.; Chiong, E. Surface Modification of Silicone with Covalently Immobilized and Cross-linked Agarose for Potential Application in the Inhibition of Infection and Omental Wrapping. *Adv. Funct. Mater.* **2014**, *24* (11), 1631−1643.

(7) Sosnin, E. A.; Stoffels, E.; Erofeev, M. V.; Kieft, I. E.; Kunts, S. E. The Effects of UV Irradiation and Gas Plasma Treatment on Living Mammalian Cells and Bacteria: A Comparative Approach. *IEEE Trans. Plasma Sci.* **2004**, *32*, 1544−1550.

(8) Parmegiani, L.; Accorsi, A.; Cognigni, G. E.; Bernardi, S.; Troilo, E.; Filicori, M. Sterilization of Liquid Nitrogen with Ultraviolet Irradiation for Safe Vitrification of Human Oocytes or Embryos. *Fertil. Steril.* **2010**, *94* (4), 1525−1528.

(9) Iwaguch, S.; Matsumura, K.; Tokuoka, Y.; Wakui, S.; Kawashima, N. Sterilization System Using Microwave and UV Light. *Colloids Surf., B* **2002**, *25* (4), 299−304.

(10) Riley, D. J.; Bavastrello, V.; Covani, U.; Barone, A.; Nicolini, C. An In-Vitro Study of the Sterilization of Titanium Dental Implants Using Low Intensity UV-Radiation. *Dent. Mater.* **2005**, *21* (8), 756−760.

(11) Ansari, I. A.; Datta, A. K. An Overview of Sterilization Methods for Packaging Materials Used in Aseptic Packaging Systems. *Food Bioprod. Process.* **2003**, *81* (1), 57−65.

(12) Guerrero-Beltr·n, J. A.; Barbosa-C·novas, G. V. Review: Advantages and Limitations on Processing Foods by UV Light. *Food Sci. Technol. Int.* **2004**, *10*, 137−147.

(13) Mori, M.; Hamamoto, A.; Takahashi, A.; Nakano, M.; Wakikawa, N.; Tachibana, S.; Ikehara, T.; Nakaya, Y.; Akutagawa, M.; Kinouchi, Y. Development of a New Water Sterilization Device with a 365 Nm UV-LED. *Med. Biol. Eng. Comput.* **2007**, *45* (12), 1237−1241.

(14) Reed, N. G. The History of Ultraviolet Germicidal Irradiation for Air Disinfection. *Public Health Rep.* **2010**, *125*, 15−27.

(15) Williams, G.; Seger, B.; Kamat, P. V. TiO_2-Graphene Nanocomposites. UV-Assisted Photocatalytic Reduction of Graphene Oxide. *ACS Nano* **2008**, *2* (7), 1487−1491.

(16) Howe, R. F.; Grätzel, M. EPR Study of Hydrated Anatase under UV Irradiation. *J. Phys. Chem.* **1987**, *91* (14), 3906−3909.

(17) Zhang, D.; Dougal, S. M.; Yeganeh, M. S. Effects of UV Irradiation and Plasma Treatment on a Polystyrene Surface Studied by IR-Visible Sum Frequency Generation Spectroscopy. *Langmuir* **2000**, *16* (10), 4528−4532.

(18) Tohge, N.; Shinmou, K.; Minami, T. Effects of UV-Irradiation on the Formation of Oxide Thin Films from Chemically Modified Metal-Alkoxides - Code: EP22. *J. Sol-Gel Sci. Technol.* **1994**, *2* (1−3), 581−585.

(19) Ouyang, M.; Yuan, C.; Muisener, R. J.; Boulares, A.; Koberstein, J. T. Conversion of Some Siloxane Polymers to Silicon Oxide by UV/Ozone Photochemical Processes. *Chem. Mater.* **2000**, *12* (6), 1591−1596.

(20) Decker, C. Light-Induced Crosslinking Polymerization. *Polym. Int.* **2002**, *51* (11), 1141−1150.

(21) Lendlein, A.; Jiang, H.; Junger, O.; Langer, R. Light-Induced Shape-Memory Polymers. *Nature* **2005**, *434* (7035), 879−882.

(22) Awokola, M.; Lenhard, W.; Löffler, H.; Flosbach, C.; Frese, P. UV Crosslinking of Acryloyl Functional Polymers in the Presence of Oxygen. *Prog. Org. Coat.* **2002**, *44* (3), 211−216.

(23) Reddy, N.; Reddy, R.; Jiang, Q. Crosslinking Biopolymers for Biomedical Applications. *Trends Biotechnol.* **2015**, *33*, 362−369.

(24) Lee, B. K.; Kim, J. J. Enhanced Efficiency of Dye-Sensitized Solar Cells by UV-O3 Treatment of TiO_2 Layer. *Curr. Appl. Phys.* **2009**, *9* (2), 404−408.

(25) Noh, Y. Y.; Kim, D. Y.; Yase, K. Highly Sensitive Thin-Film Organic Phototransistors: Effect of Wavelength of Light Source on Device Performance. *J. Appl. Phys.* **2005**, *98* (7), 074505.

(26) Snyder, P. J.; Reddy, P.; Kirste, R.; LaJeunesse, D. R.; Collazo, R.; Ivanisevic, A. Variably Doped Nanostructured Gallium Nitride Surfaces Can Serve as Biointerfaces for Neurotypic PC12 Cells and Alter Their Behavior. *RSC Adv.* **2018**, *8* (64), 36722−36730.

(27) Snyder, P. J.; Lajeunesse, D. R.; Reddy, P.; Kirste, R.; Collazo, R.; Ivanisevic, A. Bioelectronics Communication: Encoding Yeast Regulatory Responses Using Nanostructured Gallium Nitride Thin Films. *Nanoscale* **2018**, *10* (24), 11506−11516.

(28) Snyder, P. J.; Kirste, R.; Collazo, R.; Ivanisevic, A. Persistent Photoconductivity, Nanoscale Topography, and Chemical Functionalization Can Collectively Influence the Behavior of PC12 Cells on Wide Bandgap Semiconductor Surfaces. *Small* **2017**, *13* (24), 1700481.

(29) Lee, Y. V.; Tian, B. Learning from Solar Energy Conversion: Biointerfaces for Artificial Photosynthesis and Biological Modulation. *Nano Lett.* **2019**, *19*, 2189−2197.

(30) Gulyuk, A. V.; Lajeunesse, D. R.; Collazo, R.; Ivanisevic, A. Characterization of Pseudomonas Aeruginosa Films on Different Inorganic Surfaces before and after UV Light Exposure. *Langmuir* **2018**, *34* (36), 10806−10815.

(31) Wu, W.; Jin, Y.; Bai, F.; Jin, S. Pseudomonas Aeruginosa. In *Molecular Medical Microbiology*; Elsevier: 2015; pp 753−767.

(32) Hancock, R. E. W. Resistance Mechanisms in Pseudomonas Aeruginosa and Other Nonfermentative Gram-Negative Bacteria. *Clin. Infect. Dis.* **1998**, *27*, S93−S99.

(33) Yayan, J.; Ghebremedhin, B.; Rasche, K. Antibiotic Resistance of Pseudomonas Aeruginosa in Pneumonia at a Single University Hospital Center in Germany over a 10-Year Period. *PLoS One* **2015**, *10* (10), e0139836.

(34) Rolsma, S.; Frank, D. W.; Barbieri, J. T.; Rolsma, S.; Frank, D. W.; Barbieri, J. T. Pseudomonas Aeruginosa Toxins. In *The*

Comprehensive Sourcebook of Bacterial Protein Toxins; Elsevier: 2015; pp 133−160.
(35) Cheng, Y.; Feng, G.; Moraru, C. I. Micro-and Nanotopography Sensitive Bacterial Attachment Mechanisms: A Review. *Front. Microbiol.* **2019**, *10*, 191-1−191-17.
(36) Vadillo-Rodriguez, V.; Schooling, S. R.; Dutcher, J. R. In Situ Characterization of Differences in the Viscoelastic Response of Individual Gram-Negative and Gram-Positive Bacterial Cells. *J. Bacteriol.* **2009**, *191* (17), 5518−5525.
(37) Vadillo-Rodríguez, V.; Logan, B. E. Localized Attraction Correlates with Bacterial Adhesion to Glass and Metal Oxide Substrata. *Environ. Sci. Technol.* **2006**, *40* (9), 2983−2988.
(38) Mularski, A.; Wilksch, J. J.; Hanssen, E.; Strugnell, R. A.; Separovic, F. Atomic Force Microscopy of Bacteria Reveals the Mechanobiology of Pore Forming Peptide Action. *Biochim. Biophys. Acta, Biomembr.* **2016**, *1858* (6), 1091−1098.
(39) Snyder, P. J.; Kirste, R.; Collazo, R.; Ivanisevic, A. Nanoscale Topography, Semiconductor Polarity and Surface Functionalization: Additive and Cooperative Effects on PC12 Cell Behavior. *RSC Adv.* **2016**, *6* (100), 97873−97881.
(40) Bain, L. E.; Kirste, R.; Johnson, C. A.; Ghashghaei, H. T.; Collazo, R.; Ivanisevic, A. Neurotypic Cell Attachment and Growth on III-Nitride Lateral Polarity Structures. *Mater. Sci. Eng., C* **2016**, *58*, 1194−1198.
(41) Feng, P.; Mönch, I.; Harazim, S.; Huang, G.; Mei, Y.; Schmidt, O. G. Giant Persistent Photoconductivity in Rough Silicon Nanomembranes. *Nano Lett.* **2009**, *9* (10), 3453−3459.
(42) Dilger, S.; Wessig, M.; Wagner, M. R.; Reparaz, J. S.; Sotomayor Torres, C. M.; Qijun, L.; Dekorsy, T.; Polarz, S. Nanoarchitecture Effects on Persistent Room Temperature Photoconductivity and Thermal Conductivity in Ceramic Semiconductors: Mesoporous, Yolk-Shell, and Hollow ZnO Spheres. *Cryst. Growth Des.* **2014**, *14* (9), 4593−4601.
(43) Rudakowski, S. UV Light - A Powerful Tool for Surface Treatment. http://www.circuitnet.com, pp 1−6.
(44) Chen, C.; Ma, W.; Zhao, J. Semiconductor-Mediated Photodegradation of Pollutants under Visible-Light Irradiation. *Chem. Soc. Rev.* **2010**, *39*, 4206−4219.
(45) Cumpson, P.; Sano, N. Stability of Reference Masses V: UV/Ozone Treatment of Gold and Platinum Surfaces. *Metrologia* **2013**, *50* (1), 27−36.
(46) Moldovan, A.; Feldmann, F.; Krugel, G.; Zimmer, M.; Rentsch, J.; Hermle, M.; Roth-Fölsch, A.; Kaufmann, K.; Hagendorf, C. Simple Cleaning and Conditioning of Silicon Surfaces with UV/Ozone Sources. *Energy Procedia* **2014**, *55*, 834−844.
(47) Chen, X.; Shen, S.; Guo, L.; Mao, S. S. Semiconductor-Based Photocatalytic Hydrogen Generation. *Chem. Rev.* **2010**, *110* (11), 6503−6570.
(48) West, A. P.; Brodsky, I. E.; Rahner, C.; Woo, D. K.; Erdjument-Bromage, H.; Tempst, P.; Walsh, M. C.; Choi, Y.; Shadel, G. S.; Ghosh, S. TLR Signaling Augments Macrophage Bactericidal Activity through Mitochondrial ROS HHS Public Access. *Nature* **2011**, *472* (7344), 476−480.
(49) Yao, X.-H.; Min, H.; Lv, Z.-M. Response of Superoxide Dismutase, Catalase, and ATPase Activity in Bacteria Exposed to Acetamiprid. *Biomed. Environ. Sci.* **2006**, *19* (4), 309−314.
(50) Dominguez, D. C. Calcium Signalling in Bacteria. *Mol. Microbiol.* **2004**, *54*, 291−297.
(51) Ray Chowdhuri, A.; Tripathy, S.; Chandra, S.; Roy, S.; Sahu, S. K. A ZnO Decorated Chitosan−Graphene Oxide Nanocomposite Shows Significantly Enhanced Antimicrobial Activity with ROS Generation. *RSC Adv.* **2015**, *5* (61), 49420−49428.
(52) Ortiz de Orué Lucana, D.; Wedderhoff, I.; Groves, M. R. ROS-Mediated Signalling in Bacteria: Zinc-Containing Cys-X-X-Cys Redox Centres and Iron-Based Oxidative. *J. Signal Transduction* **2012**, *2012*, 1−9.
(53) Brynildsen, M. P.; Winkler, J. A.; Spina, C. S.; MacDonald, I. C.; Collins, J. J. Potentiating Antibacterial Activity by Predictably Enhancing Endogenous Microbial ROS Production. *Nat. Biotechnol.* **2013**, *31* (2), 160−165.
(54) Zurbriggen, M. D.; Carrillo, N.; Hajirezaei, M.-R. ROS Signaling in the Hypersensitive Response. *Plant Signaling Behav.* **2010**, *5* (4), 393−396.
(55) Nyström, T. Not Quite Dead Enough: On Bacterial Life, Culturability, Senescence, and Death. *Arch. Microbiol.* **2001**, *176* (3), 159−164.
(56) Guragain, M.; King, M. M.; Williamson, K. S.; Pérez-Osorio, A. C.; Akiyama, T.; Khanam, S.; Patrauchan, M. A.; Franklin, M. J. The Pseudomonas Aeruginosa PAO1 Two-Component Regulator CarSR Regulates Calcium Homeostasis and Calciuminduced Virulence Factor Production through Its Regulatory Targets CarO and CarP. *J. Bacteriol.* **2016**, *198* (6), 951−963.
(57) Sarkisova, S. A.; Lotlikar, S. R.; Guragain, M.; Kubat, R.; Cloud, J.; Franklin, M. J.; Patrauchan, M. A. A Pseudomonas Aeruginosa EF-Hand Protein, EfhP (PA4107), Modulates Stress Responses and Virulence at High Calcium Concentration. *PLoS One* **2014**, *9* (6), e98985.
(58) Díaz-Rosales, P.; Chabrillón, M.; Arijo, S.; Martinez-Manzanares, E.; Moriñigo, M. A.; Balebona, M. C. Superoxide Dismutase and Catalase Activities in Photobacterium Damselae Ssp. Piscicida. *J. Fish Dis.* **2006**, *29* (6), 355−364.
(59) Wood, N. J.; Sørensen, J. Catalase and Superoxide Dismutase Activity in Ammonia-Oxidising Bacteria. *FEMS Microbiol. Ecol.* **2001**, *38* (1), 53−58.
(60) Kobayashi, I.; Tamura, T.; Sghaier, H.; Narumi, I.; Yamaguchi, S.; Umeda, K.; Inagaki, K. Characterization of Monofunctional Catalase KatA from Radioresistant Bacterium Deinococcus Radiodurans. *J. Biosci. Bioeng.* **2006**, *101* (4), 315−321.
(61) Kirste, R.; Mita, S.; Hussey, L.; Hoffmann, M. P.; Guo, W.; Bryan, I.; Bryan, Z.; Tweedie, J.; Xie, J.; Gerhold, M.; Collazo, R.; Sitar, Z. Polarity Control and Growth of Lateral Polarity Structures in AlN. *Appl. Phys. Lett.* **2013**, *102* (18), 181913.
(62) Liu, F.; Collazo, R.; Mita, S.; Sitar, Z.; Duscher, G.; Pennycook, S. J. The Mechanism for Polarity Inversion of GaN via a Thin AlN Layer: Direct Experimental Evidence. *Appl. Phys. Lett.* **2007**, *91* (20), 203115.
(63) Collazo, R.; Mita, S.; Aleksov, A.; Schlesser, R.; Sitar, Z. Growth of Ga- and N- Polar Gallium Nitride Layers by Metalorganic Vapor Phase Epitaxy on Sapphire Wafers. In. *J. Cryst. Growth* **2006**, *287*, 586−590.
(64) Foster, H. A.; Sheel, D. W.; Sheel, P.; Evans, P.; Varghese, S.; Rutschke, N.; Yates, H. M. Antimicrobial Activity of Titania/Silver and Titania/Copper Films Prepared by CVD. *J. Photochem. Photobiol., A* **2010**, *216* (2−3), 283−289.
(65) Macvanin, M.; Hughes, D. Assays of Sensitivity of Antibiotic-Resistant Bacteria to Hydrogen Peroxide and Measurement of Catalase Activity. In *Antibiotic Resistance Protocols*, 2nd ed.; Gillespie, S. H., McHugh, T. D., Eds.; Humana Press: Totowa, NJ, 2010; pp 95−103.
(66) Foster, C. M.; Collazo, R.; Sitar, Z.; Ivanisevic, A. Aqueous Stability of Ga- and N-Polar Gallium Nitride. *Langmuir* **2013**, *29* (1), 216−220.
(67) Kruse, N.; Chenakin, S. XPS Characterization of Au/TiO_2 Catalysts: Binding Energy Assessment and Irradiation Effects. *Appl. Catal., A* **2011**, *391* (1−2), 367−376.
(68) Moulder, J. F. The Impact of the Scanning XPS Microprobe on Industrial Applications of X-Ray Photoelectron Spectroscopy. *J. Electron Spectrosc. Relat. Phenom.* **2019**, *231*, 43−49.

DOI: 10.1021/acsaelm.9b00347
ACS Appl. Electron. Mater. 2019, 1, 1641−1652